Available online at www.sciencedirect.com

jmr&t Journal of Materials Research and Technology

www.jmrt.com.br

Original Article

Green approach to corrosion inhibition of stainless steel in phosphoric acid of Artemesia herba albamedium using plant extract

M. Boudalia[a], R.M. Fernández-Domene[b], M. Tabyaoui[a], A. Bellaouchou[a], A. Guenbour[a], J. García-Antón[b,*]

[a] Laboratory of Nanotechnology, Materials and Environment, Department of Chemistry, Faculty of Science, University Mohammed V, Av. IbnBatouta, BP. 1014 Rabat, Morocco

[b] Ingeniería Electroquímica y Corrosión (IEC), Departamento de Ingeniería Química y Nuclear, ETSI Industriales, Universitat Politècnica de València, P.O. Box 22012, 46071 Valencia, Spain

ARTICLE INFO

Article history:
Received 11 July 2019
Accepted 17 September 2019
Available online 9 October 2019

Keywords:
Artemisia herba-alba
Essential oil
Corrosion
Inhibition
Stainless steel
Adsorption

ABSTRACT

Essential oil from aerial parts of *Artemisia herba-alba* from Morocco was hydrodistilled and its chemical composition oil was investigated by capillary GC and GC/MS. The major components were 1,8-cineole (35.6%) and camphor (24.1%). *Artemisia herba-alba* essential oil AHAO was tested as corrosion inhibitor of stainless steel (SS) in 1M H_3PO_4 using potentiodynamic polarization (PDP) and electrochemical impedance spectroscopy measurements (EIS) and scanning electronically microscopy (SEM) studies. The results obtained showed that the essential oil of Artemisia reduces the corrosion rate. Tafel polarization method indicates that the plant extract behaves as a mixed type inhibitor. The inhibition efficiency increased with inhibitor concentration to attain 88% at 1 $g.L^{-1}$ of oil at 298 K. Nyquist diagrams obtained from impedance studies provide results confirming the anti-corrosion effect of the studied plant. The temperature effect on the corrosion behavior of (SS) in 1M H_3PO_4 without and with AHAO at 1 $g.L^{-1}$ was studied in the temperature range from 298 to 353 K. Thermodynamic parameters suggested that the adsorption is spontaneous and exothermic process and support physical adsorption mechanism. The experimental data fits well into the Langmuir adsorption isotherm model. SEM/EDS studies provide the confirmatory evidence for the protection of (SS) by the green inhibitor. The results obtained from these methods used are in good agreement.

1. Introduction

Artemisia L. is a one of main genus of the tribe Anthemideae and also one of the largest genera of the family Asteraceae

* Corresponding author.
E-mail: jgarciaa@iqn.upv.es (J. García-Antón).

https://doi.org/10.1016/j.jmrt.2019.09.045

and is widespread in temperate areas such as South Europe, North Africa, North America, and Asia [1]. *Artemisia herba-alba* is a particular species in North Africa (located from Morocco to Egypt). *Artemisia herba-alba* called in Morroco "chih" is a dwarf shrub with a rapid growth in dry and warm climates and in muddy areas [2]. The Morocco attaches great importance to this plant, which is a great way to fight against erosion and desertification. Investigations on the medicinal properties of *Artemisia herba-alba* extracts reported anti-diabetic, leishmanicidal, antibacterial and antifungal properties [3,4]. In Morocco, sixteen chemotypes were found, and twelve of them have monoterpenes as major components of essential oils. The remaining four chemotypes, have sesquiterpene skeletons as the major fraction [5].

Phosphoric acid has been used in many industrial applications and may be in contact with a high number of chemical and petrochemical equipment. Most of this equipment is made from alloy steels that can be damaged by contact with the acidic solution. In this work we use stainless steel, which is widely used in metallurgical industries as building material because of its excellent mechanical properties and its cost-effectiveness [6]. However, it can undergo corrosion under certain environmental conditions, especially in an acidic environment.

It is imperative to protect the steel materials used in the phosphoric acid industry [7]. However, several studies [8,9] seem to have been carried out on the inhibition of corrosion of steel in phosphoric acid solutions. Corrosion inhibitors can be employed to protect steel alloys against several forms and various environments of corrosion. It is generally accepted that organic molecules inhibit corrosion by adsorption on metal surface [9–11]. Corrosion inhibitors are widely used to protect steel against corrosion: heterocyclic organic compounds contain the widespread conjugation in terms of unbound electrons of P, S, O, N and π electrons of multiple bonds, which allows them to coordinate with the orbitals (d) of the surface. These heteroatoms often exist in the form of polar functional groups and mainly participate in the adsorption process during metal-inhibiting interactions [11,12]. The existing results show that the organic inhibitors adsorbed on the metal surface, either by physical or chemical adsorption, or simultaneously, possibly form a protective layer [13–16].

The efficiency of inhibitors depends on the characteristics of the metal surface and the presence of polar groups in the inhibitor molecules that act as adsorption centers on the metal surface. The environmental risk posed by many synthetic inhibitors has become the major reason for studying the feasibility of using natural oils as corrosion inhibitors. Natural oils are biodegradable and do not contain heavy metals or other toxic compounds. The successful uses of naturally occurring substances to inhibit the corrosion of metals in acidic and alkaline environment have been reported by some research groups [17–22].

In the present work, the chemical composition of *Artemisia herba-alba* essential oil is established using GC and GC-MS. Then, the inhibition performance of *Artemisia herba-alba* was evaluated by potentiodynamic polarization and EIS measurement at different temperatures (298–353 K) and the thermodynamic parameters for both adsorption and activation processes were calculated and discussed. To study the correlation between the environment and corrosion, the variation of the temperature in this work is designed on the one hand to approach the real processes taking place in the industry and on the other hand to explain the mechanisms at the origin of the propagation of surface corrosion in a controlled environment.

2. Materials and methods

2.1. *Inhibitor*

2.1.1. *Plant material*

The aerial parts of *Artemisia herba-alba* were collected in May 2010 (full bloom) from Boulmane, Morocco (west of Morocco). Voucher specimens for this plant were deposited in the Herbarium of the Laboratory of Plants in the Scientific Institute in Rabat, Morocco. The entire plants were dried in the shade and stored in the laboratory at room temperature (25 °C).

2.1.2. *Essential oil isolation*

The essential oil was extracted by hydro-distillation (4 h) from the plant using a Clevenger type distillation apparatus (500 mL of water for 200 g plant material). Yellow oil was obtained in a yield of 2% (w/w) according to the dry material. Sodium sulfate (Na_2SO_4) was added as a drying agent to the decanted essential oil. After extraction, the essential oil was stored in a brown glass bottle tightly closed in order to protect it from light and air and maintained at a temperature of 4 °C until used.

2.1.3. *Essential oils analysis*

2.1.3.1. Gas chromatography analysis (GC-FID). GC analysis was carried out using a Perkin-Elmer Autosystem XL GC apparatus (Waltham, MA, USA) equipped with a dual flame ionization detection (FID) system and the fused-silica capillary columns (60 m × 0.22 mm I.D., film thickness 0.25 μm) Rtx-1 (polydimethylsiloxane) and Rtx-wax (polyethyleneglycol). The oven temperature was programmed from 60 °C to 230 °C at 2 °C/min and then held isothermally at 230 °C for 35 min. Injector and detector temperatures were maintained at 280 °C. Samples were injected in the split mode (1/50) using helium as a carrier gas (1 mL/min) and a 0.2 μL injection volume of pure oil. Retention indices (RI) of compounds were determined relative to the retention times of a series of n-alkanes (C5–C30) (Restek, Lisses, France) with linear interpolation using the Van den Dool and Kratz equation and software from Perkin-Elmer.

2.1.3.2. Gas chromatography mass spectrometry (GC-MS). Samples were analyzed with a Perkin-Elmer turbo mass detector (quadrupole) coupled to a Perkin-Elmer Autosystem XL equipped with the fused-silica capillary columns Rtx-1 and Rtx-wax. Carrier gas: helium (1 mL/min), ion source temperature: 150 °C, oven temperature programmed from 60 °C to 230 °C at 2 °C/min and then held isothermally at 230 °C (35 min), injector temperature: 280 °C, energy ionization: 70 eV, electron ionization mass spectra were acquired over the mass range 35–350 Da, split: 1/80, injection volume: 0.2 μL of pure oil.

Table 1 – Chemical composition of the UB6 stainless steel (wt %).

	Ni	Cr	Fe	Mo	C	Mn	Si	S	P	Others
UB6	25.09	20.77	43.97	4.39	0.0013	1.84	1.45	0.007	0.0029	2.36CU

2.1.3.3. Components identification. The identification of the essential oil constituents was based on the comparison of their retention index (RI), calculated relative to the retention times of a series of C-5 to C-30 n-alkanes, with linear interpolation, with those of our own library of authentic compounds or literature data [23,24].

2.2. Corrosion tests

2.2.1. Material and solutions

The chemical composition of the stainless steel (UB6) used in this study is given in Table 1.

The electrolyte used in this study was 1M H_3PO_4. The test solutions were freshly prepared before each experiment by adding essential oil of *Artemisia herba-alba* directly to the corrosive solution. Concentrations of essential oils were 0.4, 0.6, 0.8 and 1 g/L.

2.2.2. Electrochemical tests

Electrochemical measurements were carried out in a standard three-electrode cell with a platinum counter electrode, a saturated calomel reference electrode and the UB6 electrode as working electrode. All potentials were given versus saturated calomel electrode (SCE). In all measurements, mechanically polished electrodes were used. Polishing was carried out using successively finer grade of emery papers (600–1200 grade), then washed with distilled water and dried with blowing warm air. Electrodes were circular shaped and the exposed area of the specimens to the solution was 1 cm^2.

The experimental apparatus used for electrochemical studies was the PGZ 100 potentiostat, monitored by a PC computer and Voltamaster 4.0 software. The potential scan was carried out at a rate of 5×10^{-4} V/s over the potential range from −0.6 to 1.3 V/SCE.

Electrochemical impedance spectroscopy measurements (EIS) were conducted in the frequency range of 100 kHz–100 mHz, with an amplitude signal of 10 mV peak to peak. The impedance diagrams are given in the Nyquist representation. To study the effect of temperature, the cell was immersed in water thermostat in the temperature range of 298–353 K. During each experiment, the test solution was mixed with a magnetic stirrer.

3. Results and discussion

3.1. Essential oil composition

Twenty-four compounds were characterized and identified by GC and GC-MS, comprising 98.4% of the total oil. The identified compounds are listed in Table 2. The main constituents were 1.8-cineol (35.6%), camphor (24.1%), α-pinene (11.6%), camphene (4.9%) and β-pinene (4.1%). The essential oil consists mainly of oxygenated monoterpenes (62.0%) followed by monoterpene hydrocarbons (11.0%). The sesquiterpene hydrocarbons and oxygenated sesquiterpenes accounted only for 3.7% and 6.2% of the total oil, respectively.

Table 2 – Chemical composition of *Artemisia herba-alba* essential oil from Morocco.

N°[a]	Components	RI l[b]	RI p[c]	RI[d]	%[e]
1	Tricyclene	921	1011	927	0.2
2	α-Thujene	923	1024	932	0.1
3	α-Pinene	933	1024	936	11.6
4	Camphene	945	1069	950	4.9
5	1-Octen-3-ol	962	1441	962	0.2
6	β-Pinene	972	1112	978	4.1
7	Myrcene	982	1132	987	0.8
8	Yomogi alcool	985	1391	991	0.1
9	p-Cymene	1013	1268	1015	1.8
10	1,8-Cineole	1023	1212	1024	35.6
11	Limonene	1023	1202	1025	1.8
12	γ-Terpinene	1049	1243	1051	0.2
13	Terpinolene	1080	1281	1082	0.1
14	α -Thujone	1085	1394	1089	1.1
15	Linalol	1088	1538	1086	1.4
16	β-Thujone	1099	1434	1103	0.4
17	Camphor	1126	1510	1123	24.1
18	δ-Terpineol	1149	1659	1155	0.5
19	Borneol	1152	1689	1150	3.6
20	Terpinen-4-ol	1163	1591	1164	0.8
21	α-Terpineol	1174	1685	1176	2.9
22	Bornyl acetate	1270	1573	1270	0.5
23	E-Caryophyllene	1417	1591	1421	1.2
24	α-Humulene	1450	1661	1455	0.4
			TOTAL		98.4

[a] The numbering refers to elution order on apolar column (Rtx-1).
[b] RI *l* = retention indices on the apolar column of literature (König et al., 2001; National Institute of Standards and Technology, 2008).
[c] RI *a* = retention indices on the apolar column (Rtx-1).
[d] RI *p* = retention indices on the polar column (Rtx-Wax).
[e] Relative percentages of components (%) are calculated on GC peak areas on the apolar column (Rtx-1); values expressed are means of three parallel measurements.

An investigation in Tunisia revealed that α-thujone was observed as the dominant constituent in the essential oil of AHE [25], followed by α-thujone, camphor, chrysanthenone or trans-sabinyl acetate. The main compounds in the essential oil of AHE from Algeria were α -thujone (31.50–41.23%) and camphor (16.20–24.58%) [26], in the same country Dob et al. are found that camphor (19.4%) and trans-pinocarveol (16.9%) are the major component [27]. Dahmani-Hamzaoui and Baaliouamer revealed that, the main compound found were camphor (49.3%) and 1,8-cineole (13.4%) which are the same main compounds found in this study [28].

3.2. Effect of inhibitor concentration

3.2.1. Potentiodynamic polarization study

The polarization curves of stainless steel in 1M H_3PO_4 obtained without and with various concentrations of inhibitor are shown in Fig. 1. Electrochemical parameters such as corrosion

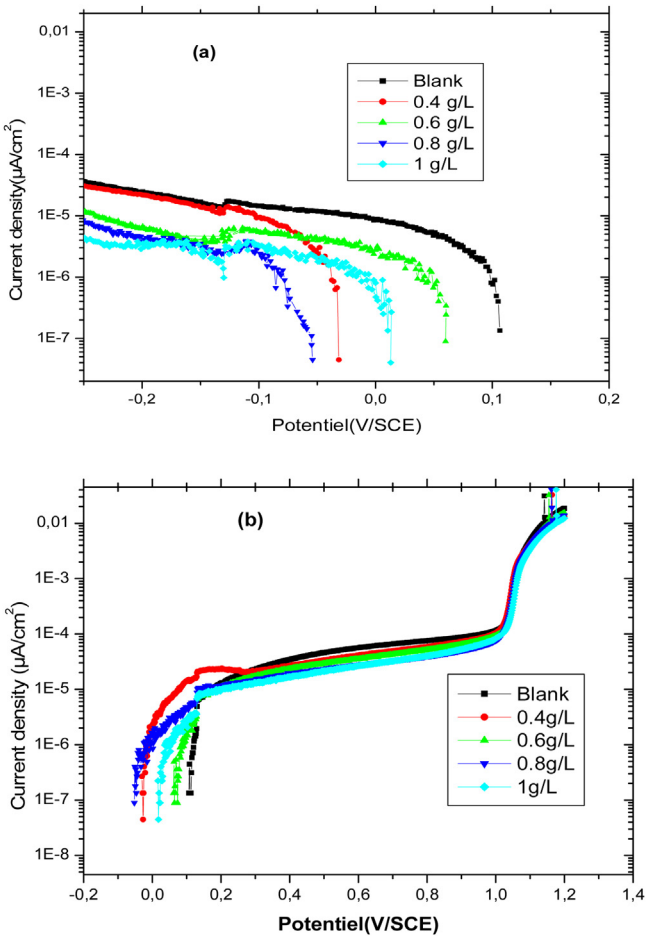

Fig. 1 – Polarization curves of stainless steel in 1M H_3PO_4 at different concentrations of AHAO.

Table 3 – Electrochemical parameters of stainless steel in 1M H_3PO_4 in the presence of different. concentrations of AHAO at 298°K.

Alloy	Blank	0.4 g.L^{-1}	0.6 g.L^{-1}	0.8 g.L^{-1}	1 g.L^{-1}
i_{corr} (μA.cm^{-2})	41.9	11.6	9.61	6.50	5.01
E_{corr} (mV/SCE)	115.1	−31.4	−65.6	−60.7	15.9
$ß_a$	295.4	430.3	271.2	353	346.2
$ß_c$	−325.7	−351.8	−941.6	−398.3	−254;8
(%)E_I	–	72.2	77.6	84.4	88.03

current density (i_{corr}), corrosion potential (E_{corr}), cathodic Tafel slope (ßc) and anodic Tafel slope (ßa) are presented in Table 3, and the inhibition efficiency *(%)* E_I of the used essential oil in 1M H_3PO_4 is also given in Table 3.

It is obvious from Fig. 1, that in the presence of inhibitor, polarization curves were shifted towards lower current values, showing the inhibition tendency of AHAO. In this case, the inhibition efficiency was calculated by using corrosion current density as follows [29]:

$$(\%)E_I = \frac{i^0_{corr} - i_{corr}}{i^0_{corr}} * 100 \quad (1)$$

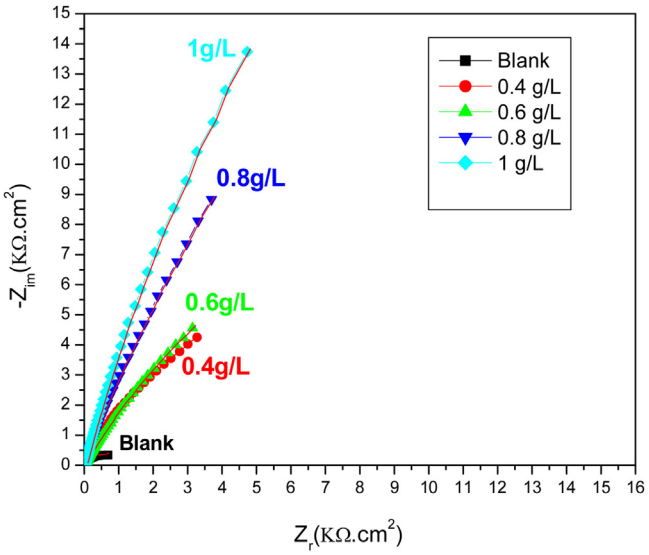

Fig. 2 – Nyquist plots for uninhibited and inhibited solution of stainless steel in phosphoric acid solution.

i_{corr} and i°_{corr} are the corrosion current density value with and without inhibitor, respectively, determined by extrapolation of cathodic Tafel lines to the corrosion potential. The data in Table 3 show that increasing the essential oil concentration decreased the corrosion current density (i_{corr}). However, it suggests that rate of electrochemical reaction was retarded due to the formation of a layer on stainless surface by adsorption of the AHAO molecules. This adsorption phenomenon might be attributed to the synergistic effect of different organic compounds of the corrosion inhibitors, this effect can be owing to an interaction between the components of the chemical composition of the inhibitor with steel surface [30] which facilitated the formation of an inhibiting film. Both the anodic and cathodic Tafel slopes, namely $ß_a$ and $ß_c$ respectively varied from the blank values. Further inspection of the table reveals that both the anodic and cathodic Tafel constants are varied with increasing extract oil concentration, which indicates the influence of the plant extract on the cathodic and anodic reactions, but the cathodic curves are more affected. On the other hand, we note that the addition of products did not change the corrosion potential values (E_{corr}) for all concentrations. This behavior indicates that the extract acted as a mixed-type inhibitor. These results led us to calculate the inhibitory efficiency *(%)*E_I which increased with the concentration of the AHAO inhibitor until reaching the maximum value of 88.03% at at 1 g.L^{-1} of AHAO.

3.2.2. *Electrochemical impedance spectroscopy*

A better understanding of the mechanisms taking place at the electrode surface was attained though EIS measurements. The EIS tests were performed under potentiostatic conditions at E_{corr} in the uninhibited and inhibited acidic solution containing various concentrations of AHAO inhibitor in 1M H_3PO_4. Nyquist and Bode plots are presented in Figs. 2 and 3, respectively.

It can be seen that in the absence and in the presence of AHAO, the Nyquist plot shows only one semicircle and there is

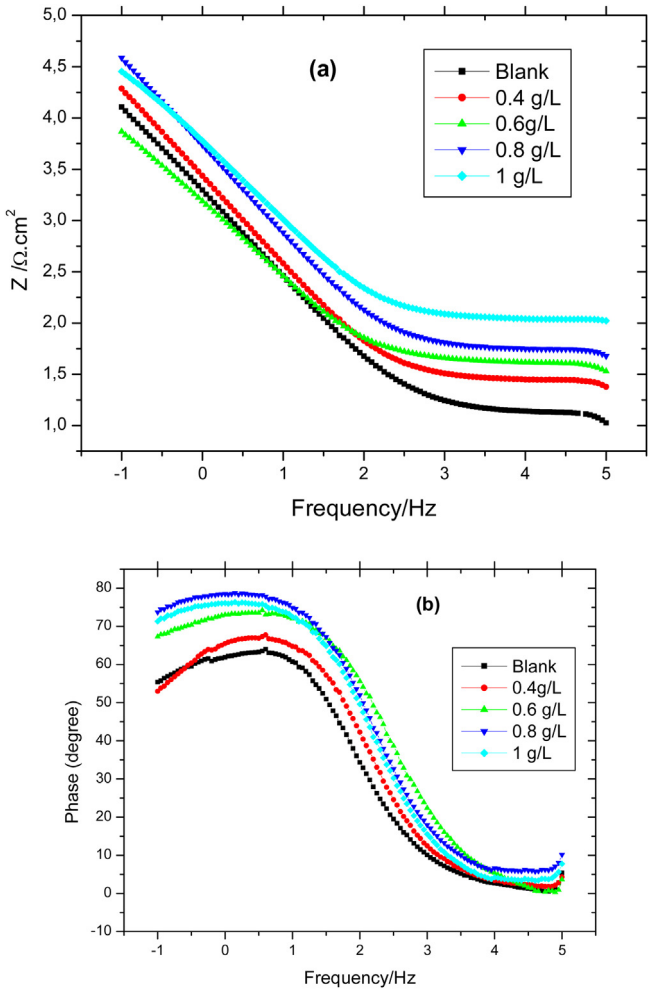

Fig. 3 – (a) Bode-module and (b) Bode-phase plots for uninhibited and inhibited solution of stainless steel in phosphoric acid solution.

only one time constant in the Bode plot. This indicates that the electrochemical process is mainly controlled by charge transfer [31]. Thus, the resistance appearing in the metal/solution interface with and without inhibitor, is the contribution of charge transfer resistance (R_{ct}). In Nyquist plot, the charge transfer resistance (R_{ct}) usually stands by difference in lower and higher frequencies in the real impedance axis. It is noted that these capacitive loops in acidic solutions are not perfect semicircles, which can be attributed to the frequency dispersion effect as a result of the roughness and inhomogeneous of electrode surface [32]. Furthermore, the diameter of the capacitive loop in the presence of inhibitor is higher than that in blank solution, and enlarges with the inhibitor concentration. This means that the impedance of the inhibited substrate increases with the inhibitor concentration, and leads to good inhibitive performance, which may be the result of an increase in the surface coverage by inhibitive molecules. This fact limits the direct access of the aggressive solution to the metal surface, hence avoiding the process of metal dissolution.

EIS data have been simulated by the proposed equivalent electrical circuit (EEC) presented in Fig. 4. In this EEC, Rs

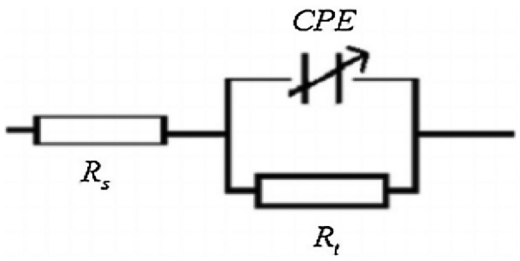

Fig. 4 – Equivalent circuit for the metal–acid interface.

Table 4 – AC impedance data of stainless steel in 1M H_3PO_4 at different concentrations of AHAO at 298°K.

	Blank	0.4 g.L^{-1}	0.6 g.L^{-1}	0.8 g.L^{-1}	1 g.L^{-1}
R_s (Ω.cm^2)	18.02	20.02	22.9	20.9	21.3
R_{ct} (kΩ.cm^2)	14.89	26.7	29.02	82.90	135.7
CPE_{dl} (μF.cm^{-2})	106	89.1	54.8	19.9	11.52
n	0.80	0.84	0.79	0.82	0.84
(%)EI	–	44.6	50	82.1	85.2

represents the solution resistance, R_{ct} represents the charge transfer resistance and *CPE* is a constant phase element representing the double layer capacitance of the interface between steel and solution, introduced to compensate for heterogeneity in the system resulting from surface roughness, impurities, dislocations, grain boundaries, adsorption of inhibitors, formation of porous layers, etc. [32,33].

The impedance function of the CPE is represented by the expression:

$$Z_{CPE} = 1/Q(jw)^n \quad (2)$$

where Q is the magnitude of the *CPE*, *j* is the imaginary number ($j^2 = -1$), *w* is the angular frequency, *n* is the deviation parameter ($-1 \leq n \leq +1$), which has the meaning of a phase shift. For $n = 0$, the *CPE* represents a pure resistor, for $n = -1$, an inductor and for $n = +1$, a pure capacitor [34]. The electric double layer can be considered as a capacitor due to its electrical properties.

The corresponding Bode plots recorded for stainless steel electrode dipped in uninhibited and inhibited solution of different concentrations of AHAO at its open circuit potential are given in Fig. 3. Bode plots are consistence with the use of an equivalent circuit containing a single constant phase element in the interface of metal/solution. The augmentation of absolute impedance at low frequencies in Bode plot confirms the higher protection with the raise of AHAO concentration [35,36].

Concerning Bode-phase plots, the increase of the phase angle with increasing AHAO concentrations indicates superior inhibitive behaviour owing to other inhibitor molecules adsorbed on steel surface at higher concentrations. The single phase peak which can be observed in Bode-phase plots, indicates that there is one time constant for the system under study, related to the electrical double layer [37].

Related parameters and corresponding data from electrochemical impedance spectroscopy measurements, such as R_s (Ω.cm^2), R_{ct} (kΩ cm^2), CPE_{dl} (μF/cm^2), *n* and (%) E_I are listed

Table 5 – The influence of temperature on the electrochemical parameters for stainless steel electrode with and without the optimum concentration of AHAO.

	1M H_3PO_4		$1g.L^{-1}$ + 1M H_3PO_4		(%)E_I
	E_{corr} (mV/SCE)	i_{corr} ($\mu A/cm^2$)	E_{corr} (mV/SCE)	i_{corr} ($\mu A/cm^2$)	
298 K	−172.6	41.9	−50	5	88
313 K	136.8	55.0	156.8	10.6	80.7
333 K	158.8	72.9	67	20.3	72.1
353 K	154.1	83.4	10.59	34.6	58.5

in Table 4. The inhibition efficiency ((%) EI) was calculated according to the following equation:

$$(\%)E_I = \frac{R_{ct} - R^{\circ}_{ct}}{R_{ct}} * 100 \quad (3)$$

Where R_{ct} and R°_{ct} are the charge-transfer resistance values with and without inhibitor, respectively

It is found from Table 4 that, as the AHAO concentration augmented, R_{ct} values increased, and the CPE_{dl} values tended to decrease. The increase in R_{ct} values is caused by adsorption of inhibitor, while the decrease in CPE_{dI}, can result from a decrease in local dielectric constant and/or an increase in the thickness of the electrical double layer. This result suggests that AHAO inhibitor act by adsorption at the metal-solution interface.

The impedance results also show that the (%) E_I increases continuously with increasing AHAO concentration and the maximum value: 85.2% was achieved in the case of $1\,gL^{-1}$. The inhibition efficiencies calculated from the EIS study show the same trend as these obtained from polarization measurements. Therefore, these results suggest, once again, that this AHAO plant extract could serve as an effective corrosion inhibitor.

3.3. *Effect of temperature*

The composition of the medium and its temperature are essential parameters affecting the phenomenon of corrosion. Electrochemical steady state measurements were taken at various temperatures. The effect of temperature in the range 293–353 K on the electrochemical parameters of stainless steel in the absence and presence of AHAO at a concentration of (1 g/L) are shown in Table 5. These results reveal that the corrosion rate of stainless steel in both free and inhibited acidic media are augmented with rising of temperature.

The inhibition efficiency of the AHAO extract decreased markedly with increasing temperature. This result supports the idea that the adsorption of extract components onto the stainless steel surface was physical in nature [38]. Thus, as the temperature increased, the number of adsorbed molecules decreased, leading to a decrease in the inhibition efficiency. This behavior is due to desorption of adsorbed inhibitor molecules from the stainless steel surface. In order to calculate activation parameters of the corrosion reaction such as activation energy E°_a, activated entropy ΔS°_a and activation enthalpy ΔH°_a for the corrosion of stainless steel in acid solution in absence and presence of different concentrations of AHAO, the Arrhenius Eq. (4) and its alternative formulation called transition state Eq. (5) were employed:

$$i_{corr} = A\ \exp\left(\frac{E^{\circ}_a}{RT}\right) \quad (4)$$

$$i_{corr} = \frac{RT}{Nh}\exp\left(\frac{\Delta S^{\circ}_a}{R}\right)\exp\left(-\frac{\Delta H^{\circ}_a}{RT}\right) \quad (5)$$

where E°_a is the apparent activation corrosion energy, T is the absolute temperature, R is the universal gas constant, A is the Arrhenius pre-exponential factor, h is he Plank's constant, N is the Avogrado's number, ΔS°_a is the entropy of activation and ΔH°_a is the enthalpy of activation. Plotting the logarithm of the corrosion rate (i) versus reciprocal of absolute temperature, the activation energy can be calculated from the slope ($-E^{\circ}_a/R$). Fig. 5a shows the variations of ln (i) with ($1/T$) in the presence and absence of inhibitor.

The logarithm of the corrosion rate of stainless steel ln (i) can be represented as straight-line functions of (10^3/T) with linear regression coefficients close to 1, indicating that the corrosion of stainless steel in phosphoric acid without and with inhibitor follows the Arrhenius equation. The activation energy (E°_a) values were calculated from the Arrhenius plots (Fig. 5a) and the results are shown in Table 6.

Furthermore, using Eq. (5), plots of Ln (i/T) versus $10^3/T$ gave straight lines (Fig. 5b) with a slope of ($-\Delta H^{\circ}_a/R$) and an intercept of ($\ln(R/Nh) + (\Delta S^{\circ}_a/R)$) from which the values of ΔH°_a and ΔS°_a were calculated and are listed in Table 6.

Analysis of the temperature dependence on inhibition efficiency as well as comparison of corrosion activation energy in the absence and presence of inhibitor give an insight knowledge on the possible mechanism of inhibitor adsorption. A decrease in inhibition efficiency with rise in temperature and with an increase in (E°_a), in the presence of inhibitor, is frequently interpreted as the formation of an adsorptive film of physisorption [39]. Previous studies have shown that, unchanged or lower values of (E°_a) in inhibited systems compared to the blank, are indicative of chemisorption mechanism, while higher values of (E°_a) suggest a physical adsorption mechanism [40].

All calculated parameters are given in Table 6. Higher values of (E°_a) in the presence of AHAO are good indication of strong inhibitive action of the plant extract by increasing the energy barrier for the corrosion process [41]. Moreover, higher values of (E°_a) in the presence of AHAO can also be correlated with the increase in thickness of the double layer that enhance the (E°_a) of the corrosion process [41,42].

Table 6 – Activation parameters, pre-exponential factor, enthalpy and entropy of dissolution reaction of Stainless steel in 1M H3PO4 containing various concentrations of extract.

C (g/L)	E_a°(Kj/mol)	ΔH_a°(Kj/mol)	$E_a^\circ - \Delta H_a^\circ$(Kj/mol)	ΔS_a°(j/mole.k)
Blank	10.14	7.47	2.67	−302.96
Blank + 1 g/L AHAO	27.50	24.83	2.67	−261.31

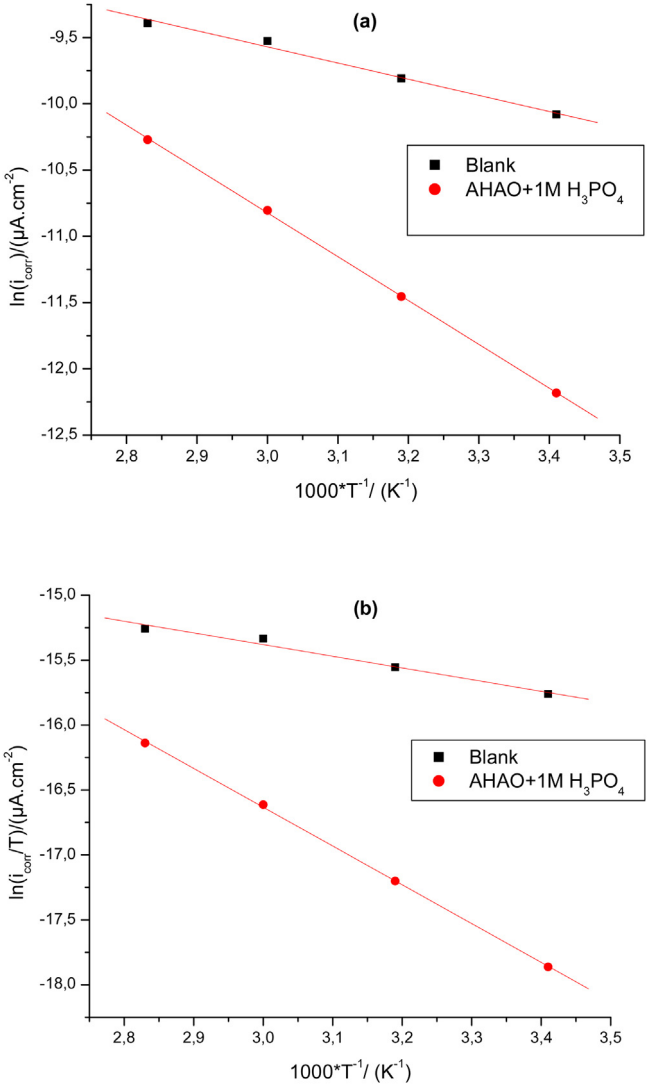

Fig. 5 – Arrhenius straight lines calculated from corrosion rate of stainless steel in 1M H_3PO_4 and 1M H_3PO_4 + 1 g L^{-1} AHAO.

The positive values of ($\Delta H^\circ a$) reflect the endothermic nature of the steel dissolution process. Negative values of ($\Delta S^\circ a$) imply that the degree of disorder increased when going from reactant to product. It is observed that the shift of ($\Delta S^\circ a$) to a more positive value when adding the concentration of the extract oil is the driving force that can overcome the barriers for the adsorption of inhibitor onto the stainless steel surface [42].

On the other hand, the average difference value of the $E^\circ{}_a - \Delta H^\circ{}_a$ is 2.67 KJ.mol^{-1}, which is approximately equal to the average value of RT (2.47 KJ.mol^{-1}) at the average temperature of the studied domain. This result agrees that the corrosion process is a unimolecular reaction as described by the known Eq. (6) of perfect gas:

$$E_a^\circ - \Delta H_a^\circ = RT \tag{6}$$

Table 7 – Parameter of Langmuir adsorption isotherm for the AHAO inhibitor.

Inhibitor	R^2	Slope	K_{ads} (L/mg)	ΔG_{ads}° (KJ/mol)
AHAO	0.99988	1.07	14,1 10^2	−23,6

3.4. *Adsorption isotherm*

The extent of corrosion inhibition mainly depends on the surface conditions and of the adsorption mode of the inhibitor. Assumptions were made that the uncovered parts of the metal surface are equal to zero and the corrosion process takes place only at this uncovered parts [43]. The degree of surface coverage (Θ) has been calculated as follows, Θ = IE/100 by assuming a direct relationship between surface coverage and inhibition efficiency as presented in Table 7.

The efficiency of this compound as a successful corrosion inhibitor mainly depends on its adsorption ability on the metal surface [44]. So, it is essential to know the mode of adsorption and the adsorption isotherm that can give valuable information on the interaction of compounds of inhibitor and metal surface. In order to better understand the mode of adsorption of the extract on the surface of the stainless steel, the surface coverage values were adjusted in some adsorption isotherms and the values of the correlation coefficient (R^2) were used to determine the best fit.

In this study, we fit the data to the Langmuir adsorption isotherm [43] as shown in Fig. 6. Plotting C_{inh}/θ versus C_{inh} yielded a straight line with a correlation coefficient (R^2) of 0.9998 and a slope close to 1. This suggests that the adsorption of AHAO on metal surface followed the Langmuir adsorption isotherm according to the following equation which is described by the mathematical form employed of the isotherm:

$$\frac{C}{\theta} = \frac{1}{K} + C \tag{7}$$

Where $\frac{C}{\theta}$ is the ratio of inhibitor concentration to surface coverage, and K is the adsorption equilibrium constant, a correlation between surface coverage (θ) obtained from polarization curves and the concentrations of AHAO (C_{inh}).

Thermodynamic parameters are important to further understand the adsorption process of inhibitor on steel/solution interface (Table 7). The equilibrium adsorption

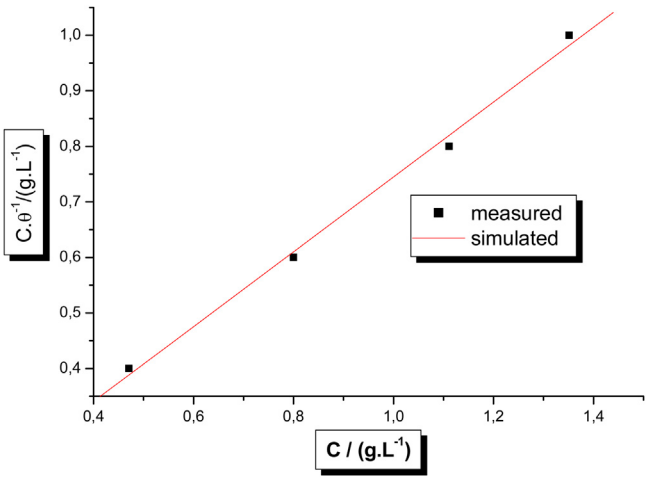

Fig. 6 – Langmuir isotherm adsorption model of AHAO on the stainless steel surface in 1M H_3PO_4.

constant, K_{ads}, is related to the standard Gibb's free energy of adsorption (ΔG°_{ads}) with the following Eq. (8):

$$\Delta G^{\circ}_{ads} = -RTLn\,(C_{H2O}.K_{ads}) \quad (8)$$

Where R is the universal gas constant, T is the thermodynamic temperature, and the value of the concentration of water in the solution is (10^3 g/L).

It is evident that linear correlation coefficients (R^2) and the slope values are also close to 1, which indicates that the adsorption of extracted oil on stainless steel surface obeys Langmuir adsorption isotherm. This result showed that the adsorbed molecules occupy only one site and there are no interactions with other adsorbed species [45].

In our studies, the negative value calculated of (ΔG°_{ads}) ensures the spontaneity of the adsorption process and stability of the adsorbed layer on metal surface [10]. It is well known that values of (ΔG°_{ads}) of -20 kJ.mol^{-1} and less negative indicate a physisorption, while those of order of -40 kJ.mol^{-1} or more negative indicate chemisorption. Thus, the (ΔG°_{ads}) value obtained here shows that in the presence of 1M H_3PO_4, physisorption of Artemisia herba alba on the stainless steel may occur [45].

3.5. *Scanning electron microscopy (SEM)*

Fig. 7 shows a state of the stainless steel surface after 1 week immersion in 1M H_3PO_4. Severe corrosion of the stainless steel is observed after immersion in the acidic solution without inhibitor (Fig. 7). There is formation of corrosion products that presumably covers the entire surface of the material. These corrosion products then form a porous layer that does not allow the protection of stainless steel, hence a severe attack is found. On the other hand, the addition of 1 g/L of AHAO of plant extract in the aggressive environment has visibly reduced the corrosive attack of stainless steel (Fig. 8). Therefore, this prevents the formation of corrosion products which

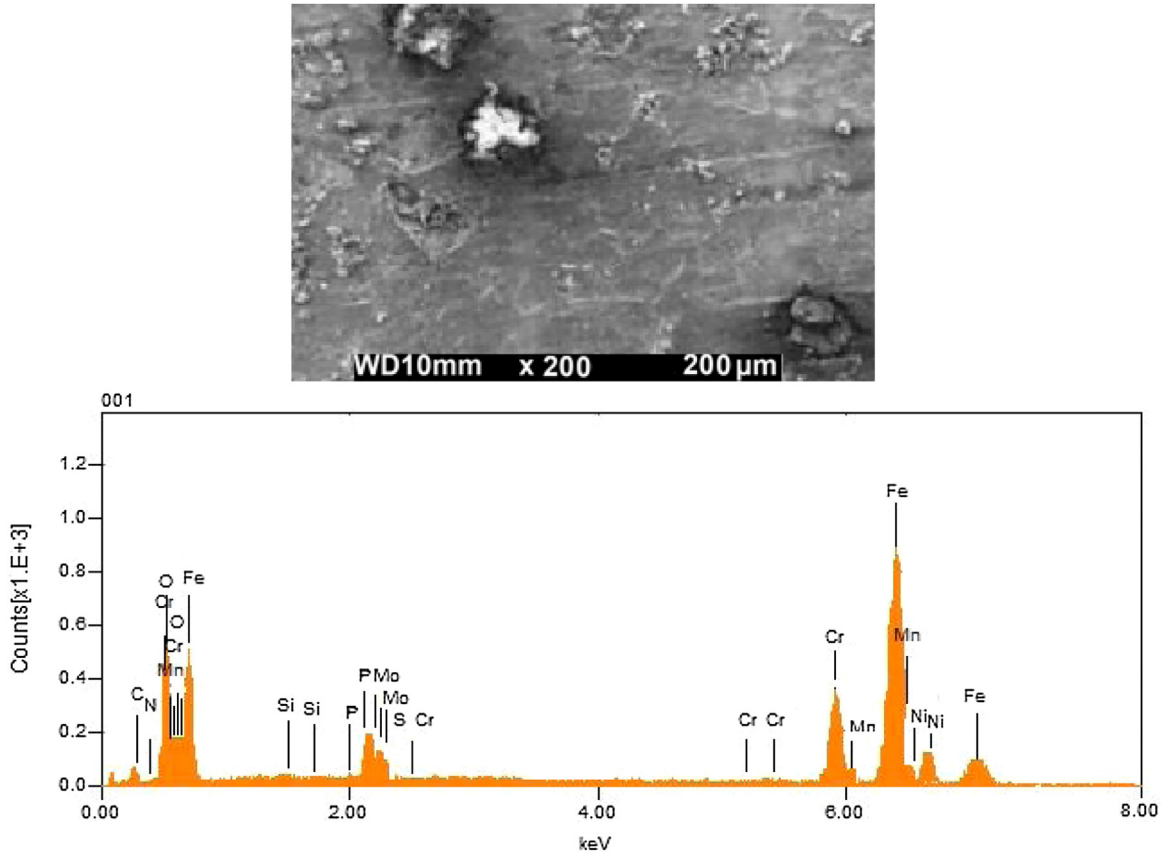

Fig. 7 – SEM/EDX image of the Stainless steel after 1 week of immersion in 1M H3PO4 without AHAO inhibitor.

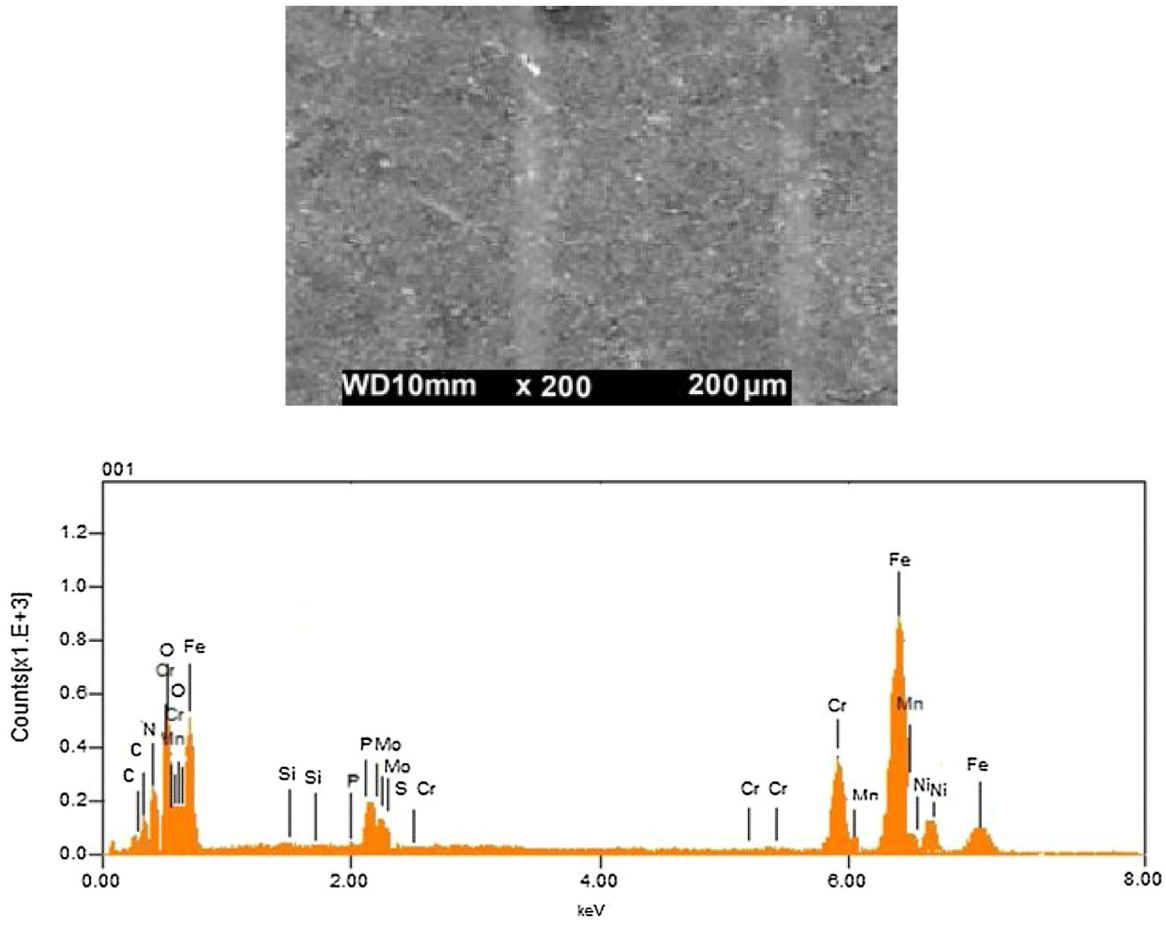

Fig. 8 – SEM image of the Stainless steel after 1 week of immersion in 1M H3PO4 with 1 g/L of AHAO inhibitor.

would lead to the deterioration of stainless steel. In addition, to determine the elemental composition in the absence and presence of essential oil on the surface of the stainless steel during the corrosion process, the EDX sounding spectra are used. Figs. 7 and 8 also show the EDX spectra for stainless steel before and after exposure to H_3PO_4 1M and H_3PO_4 1M+ 1 g/L of essential oil. It is clear from Fig. 7 that the EDX spectrum in aggressive solution (H_3PO_4 1M) presents the characteristic peaks of certain elements contained in the chemical composition of the surface of the electrode. Then, in the presence of essential oil, the appearance of the characteristic peak of nitrogen as well as an increase in the intensity of the peaks of oxygen and carbon can be observed, which are present in the chemical composition of the essential oil.

4. Conclusions

On the basis of these results, the following conclusions may be drawn:

- The AHAO tested reveal excellent protective qualities for protection of stainless steel against corrosion in 1M H_3PO_4 medium, and the inhibition efficiency increases with increase in the inhibitor concentration.
- Based on the Tafel polarization results, the compounds can be classified as mixed-type inhibitor. The inhibition efficiency increased with increasing inhibitor concentrations to attain a maximum value of 88.03% for inhibitor AHAO at 1 $g.L^{-1}$.
- EIS measurements depicted an increase in charge transfer resistance (R_{ct}) and a decrease in constant phase element representing double layer capacitance (CPE_{dl}) in the presence of AHAO that suggest the adsorption of these molecules on the surface of the stainless steel.
- The inhibiting action of this essential oil can be attributed to the adsorption via the synergistic effect of the majority constituents as well as the minor components of the composition of the AHAO inhibitor.
- The inhibition efficiency decreased with increasing temperature as a result of the higher dissolution of stainless steel at higher temperature.
- The value of apparent activation energy increased with the increase in the inhibitor concentration. Enthalpy of activation reflects the endothermic nature of the stainless steel dissolution process. Entropy of activation increased with increasing inhibitor concentration, hence implicating an increase in the degree of disorder of the system.
- The adsorption of the tested inhibitor on interface between the stainless steel and phosphoric acid obeys the Langmuir adsorption isotherm model.

- Gibbs free energy of adsorption, enthalpy of adsorption and entropy of adsorption indicated that the adsorption process is spontaneous and exothermic and that the molecules adsorbed on the metal surface by the process of physical adsorption.
- SEM/EDX studies reveal the protection of the metal from corrosion in acid medium by Artemisia herba alba.

Conflicts of interest

There are no conflicts of interest for any authors.

REFERENCES

[1] El Ouariachi EM, Tomi P, Bouyanzer A, Hammouti B, Desjobert JM, Costa J, et al. Chemical composition and antioxidant activity of essential oils and solvent extracts of Ptychotis verticillata from Morocco. Food Chem Toxicol 2011;49(2):533–6, http://dx.doi.org/10.1016/j.fct.2010.11.019.

[2] Belhattab R, Amor L, Barroso JG, Pedro LG, Cristina Figueiredo A. Essential oil from Artemisia herba-alba Asso grown wild in Algeria: variability assessment and comparison with an updated literature survey. Arab J Chem 2014;7(2):243–51, http://dx.doi.org/10.1016/j.arabjc.2012.04.042.

[3] Tilaoui M, Ait Mouse H. Comparative phytochemical analysis of essential oils from different biological parts of Artemisia herba alba and their cytotoxic effect on cancer cells. PLoS One 2015;10(7):e0131799, http://dx.doi.org/10.1371/journal.pone.0131799.

[4] (a) Uko MS, Usman A, Toma I, Okhale SO, Magili ST, Adzu B. Evaluation of active phytochemical constituents linked to the analgesic and anti-inflammatory property of Cassia singueana Del root bark. J Medic Plant Res 2019;13(12):288–95, http://dx.doi.org/10.5897/JMPR2019.6776; (b) Lopes-Lutz D, Alviano DS, Alviano CS, Kolodziejczyk PP. Screening of chemical composition, antimicrobial and antioxidant activities of Artemisia essential oils. Phytochemistry 2008;69(8):1732–8, http://dx.doi.org/10.1016/j.phytochem.2008.02.014.

[5] Haouari M, Ferchichi A. Essential oil composition of Artemisia herba-alba from Southern Tunisia. Molecules 2009;14(4):1585–94, http://dx.doi.org/10.3390/molecules14041585.

[6] Messali M, Lgaz H, Dassanayake R, Salghi R, Jodeh S, Abidi N, et al. Guar gum as efficient non-toxic inhibitor of carbon steel corrosion in phosphoric acid medium: electrochemical, surface, DFT and MD simulations studies. J Mol Struct 2017;1145(9):43–54, http://dx.doi.org/10.1016/j.molstruc.2017.05.08194.

[7] Musa AY, Kadhum AAH, Takriff MS, Daud AR, Kamarudin SK, Muhamad N. Corrosion inhibitive property of 4-amino-5-phenyl-4H-1, 2, 4-triazole-3-thiol for mild steel corrosion in 10M hydrochloric acid. Corros Eng Sci Technol 2010;45(2):163–8, http://dx.doi.org/10.1179/147842208X386359.

[8] Li XH, Deng SD, Xie XG. Inhibition effect of tetradecylpyridinium bromide on the corrosion of cold rolled steel in 7.0 m H3 PO4. Arabian J Chem 2017;10:S3715–24, http://dx.doi.org/10.1016/j.arabjc.2014.05.004.

[9] Zarrok H, Zarrouk A, Salghi R, Hammouti B, Elbakri M, Touhami M, et al. Study of a cysteine derivative as a corrosion inhibitor for carbon steel in phosphoric acid solution. Res Chem Intermed 2014;40(2):801–15, http://dx.doi.org/10.1007/s11164-012-1004-0.

[10] Wang L, Zhu MJ, Yang FC, Gao CW. Study of a triazole derivative as corrosion inhibitor for mild steel in phosphoric acid solution. Int J Corros Scale Inhib 2012;2012:1–6, http://dx.doi.org/10.1155/2012/573964.

[11] Ouachikh O, Bouyanzer A, Bouklah M, Desjobert JM, Cost J, Hammouti B, et al. Application of Essential oil of Artemisia Herba Alba as green corrosion inhibitor for steel in 0.5 M H_2SO_4. Sur Rev Lett 2009;16(1):49–54, http://dx.doi.org/10.1142/s0218625x09012287.

[12] Lucatero LMB, Ortega DT, Pandiyan T, Singh N, Singh H, Sarao TPS. Corrosion inhibition studies of cigarette waste on the iron surface in acid medium: electrochemical and surface morphology analysis. Anti Corros Method M 2016;63(4):245–55, http://dx.doi.org/10.1108/ACMM-05-2014-1384.

[13] Ambrish S, Ansari KR, Quraishi MA, Kaya S, Banerjee P. The effect of an N-heterocyclic compound on corrosion inhibition of J55 steel in sweet corrosive medium. New J Chem 2019;43:6303–13, http://dx.doi.org/10.1039/C9NJ00356H.

[14] Chakravarthy MP, Mohana KN, Kumar PCB. Corrosion inhibition effect and adsorption behaviour of nicotinamide derivatives on mild steel in hydrochloric acid solution. Int J Ind Chem 2014;5(2):1–21, http://dx.doi.org/10.1007/s40090-014-0019-3.

[15] Caroline AI, Abdulrahaman AS, Kobe IH, Ganiyu KA, Adams SM. Inhibitive performance of bitter leaf root extract on mild steel corrosion in sulphuric acid solution. Am J Mater Eng Technol 2015;3(2):35–45, http://dx.doi.org/10.12691/materials-3-2-3.

[16] Martinez S. Inhibitory mechanism of mimosa tannin using molecular modeling and substitutional adsorption isotherms. Mater Chem Phys 2003;77(1):97–102, http://dx.doi.org/10.1016/s0254-0584(01)00569-7.

[17] Ajani KC, Abdulrahman AS, Mudiare E. Inhibitory action of aqueous citrus aurantifolia seed extract on the corrosion of mild steel in H2SO4 solution. World Appl Sci J 2014;31(12):2141–7, http://dx.doi.org/10.5829/idosi.wasj.2014.31.12.711.

[18] Abdulahman AS, Ismail M. Evaluation of corrosion inhibiting admixtures for steel reinforcement in concrete. Int J Phys Sci 2012;7(1):139–43, http://dx.doi.org/10.5897/IJPS11.966.

[19] Ouachikh O, Bouyanzer A, Bouklah M, M-Desjobert J, Costa J, Hammouti B, et al. Application of essential oil of artemisia herba alba as green corrosion inhibitor for steel in 0.5 m H_2SO_4. Surf Rev Lett 2009;16(1):49–54, http://dx.doi.org/10.1142/S0218625X09012287.

[20] Ostovari A, Hoseinieh SM, Peikari M, Shahizadeh SR, Hashemi SJ. Corrosion inhibition of mild steel in 1 M HCL solution by henna extract: a comparative study of the inhibition by henna and its constituents (lawsone, gallic acid, α-D-glucose and tannic acid). Corros Sci 2009;51(9):1935–49, http://dx.doi.org/10.1016/j.corsci.2009.05.024.

[21] Prabakaran M, Kim SH, Sasireka A, Kalaiselv IK, Chung IM. Polygonatum odaratum extract as an eco-friendly inhibitor for aluminum corrosion in acidic medium. J Adhes Sci Technol 2018;32(18):2054–69, http://dx.doi.org/10.1080/01694243.2018.1462947.

[22] El-Etre AY. Khillah extract as inhibitor for acid corrosion of SX 316 steel. Appl Surf Sci 2006;252(24):8521–5, http://dx.doi.org/10.1016/j.apsusc.2005.11.066.

[23] Hazwan MH, Jain KM. The corrosion inhibition and adsorption behavior of Uncaria gambir extract on mild steel in 1 M HCl. Mater Chem Phys 2011;125(3):461–8, http://dx.doi.org/10.1016/j.matchemphys.2010.10.032.

[24] Laribi B, Kouki K, Mougou A, Marzouk B. Fatty acid and essential oil composition of three Tunisian caraway (Carum carvi L.) seed ecotypes. J Sci Food Agric 2010;90(3):391–6, http://dx.doi.org/10.1002/jsfa.3827.

[25] Chaieb I, BenHamouda A, Tayeb W, Zarrad K, Bouslema T, Laarif A. The Tunisian Artemisia essential oil for reducing contamination of stored cereals by Tribolium castaneum. Food Technol Biotech 2018;56(2):247–56, http://dx.doi.org/10.17113/ftb.56.02.18.5414.
[26] Benabdellah M, Benkaddour M, Hammouti B, Bendahhou M, Aouiniti A. Inhibition of steel corrosion in 2M H_3PO_4 by Artemisia oil. Appl Surf Sci 2005;252(18):6212–7, http://dx.doi.org/10.1016/j.apsusc.2005.08.030.
[27] Dob T, Benabdelkader T. Chemical composition of the essential oil of Artemisia herba-alba asso grown in Algeria. J Essent Oil Res 2006;18(6):685–90, http://dx.doi.org/10.1080/10412905.2006.9699206.
[28] Dahmani-Hamzaoui N, Baaliouamer A. Chemical composition of Algerian Artemisia herba-alba essential oils isolated by microwave and hydrodistillation. J Essent Oil Res 2010;22(6):514–7, http://dx.doi.org/10.1080/10412905.2010.9700386.
[29] Saxena A, Prasad D, Haldhar R. Investigation of corrosion inhibition effect and adsorption activities of Achyranthes aspera extract for mild steel in 0.5 M H_2SO4. J Fail Anal Prev 2018;18(4):957–68, http://dx.doi.org/10.1007/s11668-018-0491-8.
[30] Oguzie EE, Li Y, Wang FH. Effect of surface nanocrystallization on corrosion and corrosion inhibition of low carbon steel: synergistic effect of methionine and iodide ion. Electrochim Acta 2007;52(24):6988–96, http://dx.doi.org/10.1016/j.electacta.2007.05.023.
[31] Alagta A, Felhősi I, Bertóti I, Kálmán E. Corrosion protection properties of hydroxamic acid self-assembled monolayer on carbon steel. Corros Sci 2008;6(50):1644–9, http://dx.doi.org/10.1016/j.corsci.2008.02.008.
[32] Li X, Xie X, Deng S, Du G. Two phenylpyrimidine derivatives as new corrosion inhibitors for cold rolled steel in hydrochloric acid solution. Corros Sci 2014;87:27–39, http://dx.doi.org/10.1016/j.corsci.2014.05.017.
[33] Qian B, Hou B, Zheng M. The inhibition effect of tannic acid on mild steel corrosion in seawater wet/dry cyclic conditions. Corros Sci 2013;72:1–9, http://dx.doi.org/10.1016/j.corsci.2013.01.040.
[34] Hosseini M, Mertens SFL, Ghorbani M, Arshadi MR. Asymmetrical Schiff bases as inhibitors of mild steel corrosion in sulphuric acid media. Mater Chem Phys 2003;78(3):800–8, http://dx.doi.org/10.1016/S0254-0584(02)00390-5.
[35] Hegazy MA, Abdallah M, Awad MK, Rezk M. Three novel di-quaternary ammonium salts as corrosion inhibitors for API X65 steel pipeline in acidic solution: part I: experimental results. Corros Sci 2014;81:54–64, http://dx.doi.org/10.1016/j.corsci.2013.12.010.
[36] Xu B, Yang W, Liu Y, Yin X, Gong W, Chen Y. Experimental and theoretical evaluation of two pyridinecarboxaldehyde thiosemicarbazone compounds as corrosion inhibitors for mild steel in hydrochloric acid solution. Corros Sci 2014;78:260–8, http://dx.doi.org/10.1016/j.corsci.2013.10.007.
[37] Awad MK, Mohamed R, Mustafa B, Mohamed M, Abo Elnga B. Computational simulation of the molecular structure of some triazoles as inhibitors for the corrosion of metal surface. J Mol Struct 2010;959(1):66–74, http://dx.doi.org/10.1016/j.theochem.2010.08.008.
[38] Tiwari M, Gupta VK, Singh RA, Ji G, Prakash R. Donor−π–acceptor-type configured, dimethylamino-based organic push–pull chromophores for effective reduction of mild steel corrosion loss in 1 M HCl. ACS Omega 2018;3(4):4081–93, http://dx.doi.org/10.1021/acsomega.8b00083.
[39] Khadom AA, Yaro AS, AlTaie AS, Kadum AAH. Electrochemical, activations and adsorption studies for the corrosion inhibition of low carbon steel in acidic media. Portug Electroch Acta 2009;27(6):699–712, http://dx.doi.org/10.4152/pea.200906699.
[40] El-Etre AY. Inhibition of acid corrosion of carbon steel using aqueous extract of olive leaves. J Colloid Interface Sci 2007;314(2):578–83, http://dx.doi.org/10.1016/j.jcis.2007.05.077.
[41] Garai S, Jaisankar P, Singh JK, Elango A. A comprehensive study on crude methanolic extract of artemisia pallens (Asteraceae) and its active component as effective corrosion inhibitors of mild steel in acid solution. Corros Sci 2012;60:193–204, http://dx.doi.org/10.1016/j.corsci.2012.03.036.
[42] Awad MI. Eco friendly corrosion inhibitors: inhibitive action of quinine for corrosion of low carbon steel in 1 m HCl. J Appl Electrochem 2006;36(10):1163–8, http://dx.doi.org/10.1007/s10800-006-9204-1.
[43] Mohan R, Joseph A. Corrosion protection of mild steel in hydrochloric acid up to 313 K using propyl benzimidazole: electroanalytical, adsorption and quantum chemical studies. Egypt J Pet 2018;27(1):11–20, http://dx.doi.org/10.1016/j.ejpe.2016.12.003.
[44] Laamaria MR, Benzakour J, Berrekhis F, Derjaa A, Villemin D. Adsorption and corrosion inhibition of carbon steel in hydrochloric acid medium by hexamethylenediamine tetra(methylene phosphonic acid). Arab J Chem 2016;9(1):S245–51, http://dx.doi.org/10.1016/j.arabjc.2011.03.018.
[45] Ahamad I, Prasad R, Quraish MA. Experimental and theoretical investigations of adsorption of fexofenadine at mild steel/hydrochloric acid interface as corrosion inhibitor. J Solid State Electrochem 2010;14(11):2095–105, http://dx.doi.org/10.1007/s10008-010-1041-9.